Journal of Interfaces, Thin films, and Low dimensional systems 2 (2) Winter and Spring (2019) 157-165

Experimental aspects of α, β angles distortion on superconductivity in 1111-type Iron-based superconductor

Vahid Daadmehr *, Zahra Alborzi, and Fatemeh Shahbaz Tehrani

Magnet & superconducting Res. Lab., Department of Physics, Alzahra University, Tehran, 199389, I.R. Iran

ARTICLE INFO

Article history:
Received 31 January 2019
Revised 4 May 2019
Accepted 11 August 2019
Available online 12 Feb 2020

Keywords:
Iron based Superconductor
Doping
Superconductivity transition-temperature
Bond length and angles-of tetrahedron Structure
FeAs4- tetrahedron

ABSTRACT

In this research, we aim to clarify the relationship between the structural distortion due to doping and the superconductivity existence in the FeAs4 structure. For this, we have prepared polycrystalline of $NdFeAsO_{0.8}F_{0.2}$, $NdFeAs_{0.95}Sb_{0.05}O_{0.8}F_{0.2}$ and $Nd_{0.99}Ca_{0.01}FeAsO_{0.8}F_{0.2}$ samples by one-step solid state reaction method. The structural and electrical properties of the samples were characterized through the X-ray diffraction pattern and the 4-probe method, respectively. The XRD patterns, refined using the MAUD software and Rietveld's method, have indicated formation of the tetragonal structure with the space group P4/nmm:2. The variation of the lattice structural parameters for the $NdFeAsO_{0.8}F_{0.2}$ doping with Sb and Ca ions were obtained by the Rietveld refinement. The changes of bond lengths and the α, β bond angles have been specified from the corresponding value of α and β regular FeAs4-tetrahedron with the Sb/As and Ca/Nd doping, where they affect the superconductivity existence. The α and β bond angles increase and decrease with the substitution of Sb/As and Ca/Nd doping, which leads to the contraction of the FeAs layer, and therefore the lattice parameter "c" decreases. The superconducting transition temperature was reduced from 56K for $NdFeAsO_{0.8}F_{0.2}$ sample to 48K and 46K for Ca/Nd and Sb/As doping, respectively. It can be concluded from the structural and electrical properties that the superconducting transition temperature decreases with increasing the distortion of FeAs4-tetrahedron from the regular one. So, there is a relation between the structural properties and the superconductivity in the iron based superconductors-1111 regardless of the doping procedures.

1 Introduction

Following the discovery of Iron-based superconductors (IBs) in LaOFeP compound at $T_c = 3.2K$ by Kamihara et al. in 2006 [1], many researchers and physicists focused on this category of superconductors. They were known as high temperature superconductors, after the report of superconductivity at 26K in $LaFeAsO_{1-x}F_x$ [2]. They have a layered structure like cuprate superconductors, the small anisotropy, the large upper critical field, the advantageous grain boundary nature and the multi-

*Corresponding author.
Email address: Daadmehr@Alzahra.ac.ir
DOI: 10.22051/jitl.2019.24394.1026

band nature of Fe-3d [1, 3-6]. There are six subgroups for these types of superconductors: $FeSe_{1-x}Te_x$ (11-type) [7], LiFeAs (111-type)[8], MFe_2As_2 (122-type) that M=Ba, Sr, K [9, 10], ReFeAsO (1111-type) that Re= rare earth element atoms [11-13], $MFeAs_2$ (112-type) that M=Ca, La [14] and $A_2Fe_4Se_5$ (245-type) that A = K, Rb, Cs [15]. The 1111-type shares the honor with the highest superconductivity transition temperature (T_C), in all types of the IBs [16-20].

The electron doping and hole doping change the T_C of IBs where the effect of these substitutions is the most interesting subject regarding thier electrical and structural properties. We consider two doping procedures: i) substitution in superconductive planes of FeAs (as mentioned in Ref.[21]), ii) substitution in Re (O, F) layer of charge reservoirs (as mentioned in Ref. [18]).

Among the types of 1111, the nominal composition $NdFeAsO_{0.8}F_{0.2}$ has the highest T_C [16]; therefore, we selected this compound to investigate the effect of substitutions on the superconductive plane of FeAs and charge reservoirs Nd(O,F).

In this work for the first time, we study the effects of Ca and Sb substitutions on polycrystalline $Nd_{1-x}Ca_xFeAs_{1-y}Sb_yO_{0.8}F_{0.2}$ with x=0.0, 0.01 and y=0.0, 0.05, synthesized through one step solid-state reaction method. Specifically, we analyze the structural properties of these samples via X-ray diffraction pattern (XRD) by refined with the Rietveld's method with the MAUD software. We argue about the effect of structural properties such as bond angles, bond length of FeAs plane on the T_C of the nominal composition $NdFeAsO_{0.8}F_{0.2}$. The purpose of this research is to investigate the relationship between the structural and superconducting properties of the 1111-type of IBs that are doped by the calcium and antimony, regardless of whether the doping is in the superconductive planes of FeAs, or in Re (O, F) layer of charge reservoirs, and regardless of the doping type (calcium is hole dopant, and in the case of antimony, the doping is an isovalent of As element).

2 Materials and methods

2.1 Synthesis methods

Samples with nominal compositions of $Nd_{1-x}Ca_xFeAs_{1-y}Sb_yO_{0.8}F_{0.2}$ with x=0.0, 0.01 or y=0.0, 0.05 labeled as Nd-1111 for x, y=0.0, Nd-Ca0.01 for x=0.01, y=0.0 and Nd-Sb0.05 for x=0.0, y=0.05, were prepared by one step solid-state reaction method, based on Alborzi et al. [16]. The Neodymium powder (99.99%), Arsenic pieces (99.99%), Fe_2O_3 (99.9%), FeF_3 (99%), Fe (99.99%), CaF_2 (99%), and Sb (99.5%) powders were used as precursor materials. The stoichiometric amounts of these powders were mixed and grounded for 2 hours. All the processes were carried out in a glove box with Nitrogen atmosphere. The homogenous mixtures were pressed into pellets and were sealed in the evacuated quartz tubes. Then, the sealed and evacuated quartz tube was heated with a slow heating rate through 4 stages: (i) 5 h at 350 °C, (ii) 14 h at 640 °C, (iii) 20 h at 880 °C, and (iv) 20 h at 1150 °C. After the heat treatment, the sample comes in powder form in the quartz tube. Again, the powder was pressed and was encapsulated in an evacuated quartz tube. The heat treatment was repeated.

2.2 Characterization

The X-ray diffraction patterns (XRD) of the synthesized samples were performed using a PANalytical® PW3050/60 X-ray diffractometer with Cu-Kα radiation (λ= 1.54056Å) operated at 40kV and 40mA with a step size of 0.026°. The refinement method of Rietveld was applied with the "Material Analysis Using Diffraction" (MAUD) program (v.2.8). The morphology of the samples was observed by TESCAN® – Mira III and VEGA3 LMU Field Emission Scanning Electron Microscope (FE-SEM). We used the 4-probe contact method for obtaining the superconductivity parameters of our samples. The 20 K Closed Cycle Cryostat (QCS 101), ZSP Croygenics Technology (Iran), was used for measurement of the superconductivity behavior of the samples.

3 Results and Discussion

3.1 Structural studies

The XRD patterns of the Nd-1111, Nd-Sb0.05 and Nd-Ca0.01 have been showed in Figure 1. For the structural analysis, the X-ray diffraction data of our synthesized samples have been refined by using the MAUD software with the Rietveld's method. The goodness of fit (S) is described by $S= R_{wp} /R_{exp}$, where R_{wp} is the weighted residual error while R_{exp} is the expected error. These parameters are listed in Table 1 which demonstrate that the refinement quality of our samples is good. As shown in Figure 1, for the Nd-1111 sample, the existence of the major Bragg peaks in the XRD pattern confirms the formation of tetragonal structure with the P4/nmm:2 space group which indicates that almost any impurity phase is in this sample. The other two samples also have a tetragonal structure with the P4/nmm:2 space group. In addition, in the refinements, impurity phases have been included (1.5 wt% NdF_2, 0.5wt% Sb in the Nd-Sb0.05 sample and 8.7 wt% NdOF, 4.5 wt% Nd_2O_3, 9.8 wt% FeAs in the Nd-Ca0.01).

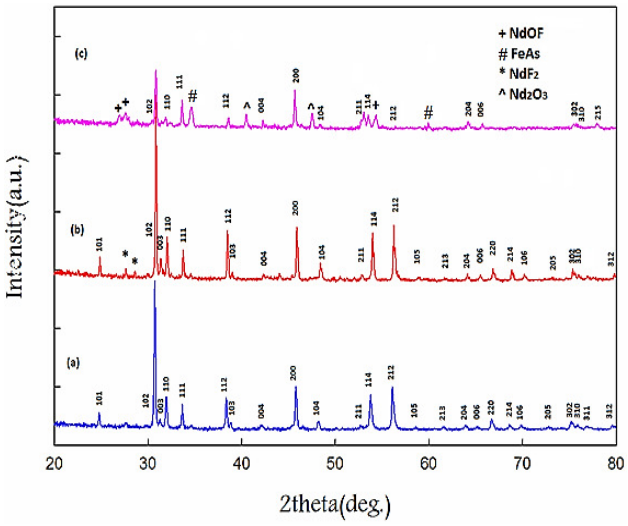

Figure 1. XRD patterns of samples: (a) Nd-1111 (blue line), (b) Nd-Sb0.05 (red line) and Nd-Ca0.01 (pink line).

Based on the MAUD analysis, Table 1 displays the real values and refined experimental values of ion positions, occupancy number, and quantity of the ions in a unit cell of the synthesized samples.

Table 1. The parameters for the calculation of pattern fitness for the synthesized samples.

composition	R_{wp} (%)	R_p (%)	R_{exp} (%)	S
$NdFeAsO_{0.8}F_{0.2}$	4.55(3)	3.48(0)	3.91(8)	1.16(2)
$Nd_{0.99}Ca_{0.01}FeAsO_{0.8}F_{0.2}$	6.00(1)	4.64(3)	3.21(4)	1.86(7)
$NdFeAs_{0.95}Sb_{0.05}O_{0.8}F_{0.2}$	5.40(2)	3.98(4)	3.56(9)	1.51(3)

It is evident from Table 2 that the calcium ions in neodymium sites and antimony ions in arsenic site are substituted completely. The XRD patterns of the synthesized samples that are refined by the MAUD software are presented in Figures 2a-2c.

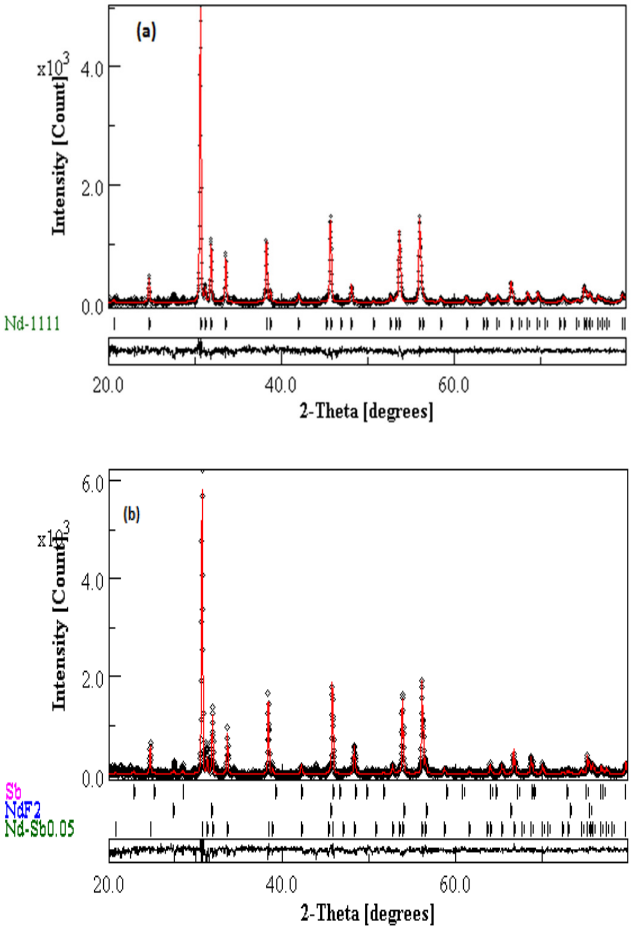

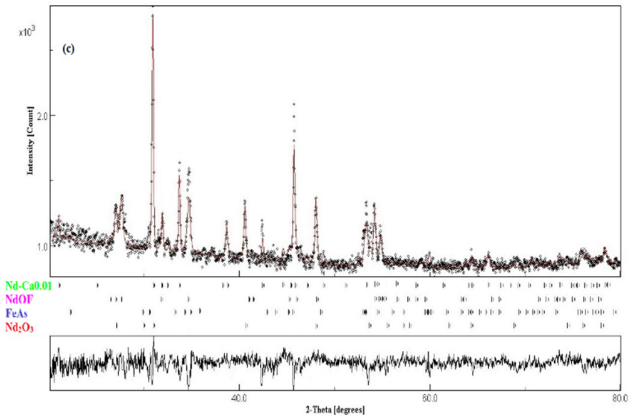

Figure 2. X-ray powder diffraction pattern and best-fit refinement profile of (a) Nd-1111, (b) Nd-Sb0.05, (c) Nd-Ca0.01, observed at room temperature. The calculated pattern is shown by a red line passing though black data points in the upper portion. The short vertical black bars below the pattern indicate the positions of the allowed reflections. The black line in the lower portion shows the differences between the observed and calculated patterns.

Figure 3 shows the crystal structure of Nd-1111 with tetragonal structure. The obtained structural parameters such as lattice parameters, bond angles, bond lengths, and the thickness of the layers by using the MAUD software are listed in Table 4. It is understood that the lattice parameter "a" is almost constant by substitution of Ca^{2+}/Nd^{3+} and Sb/As ions, but the lattice parameter "c" and the cell volume decline. This is due to the electronegativity of the doping atoms, as mentioned in ref. [22, 25, 26].

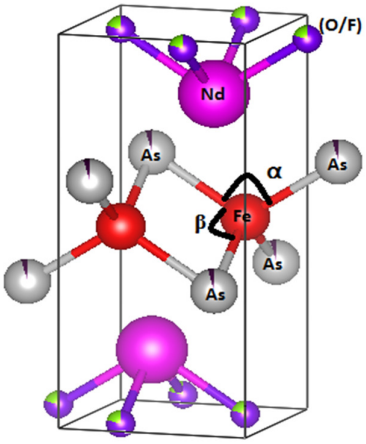

Figure 3. Schematic image of crystal structure of Nd-1111.

The electronegativity of doped ions is smaller than the electronegativity of As and Nd ions because (i) the As-Fe-As bond angles ("α" and "β") change, (ii) the bond length of Fe-As in the doped samples is less than the bond length of Fe-As in the Nd-1111 structure.

Table 2. Structural parameters before and after refinement from MAUD analysis for the synthesized samples.

Sample	**Structural parameters before refinement**				
	Ions	Position			Occupancy
		x	y	z	
$NdFeAsO_{0.8}F_{0.2}$	Nd^{3+}	0.25	0.25	0.138(5)	1
	Fe^{2+}	0.75	0.25	0.5	1
	As	0.25	0.25	0.65(7)	1
	O^{2-}	0.75	0.25	0	0.8
	F^{-}	0.75	0.25	0	0.2
$Nd_{0.99}Ca_{0.01}FeAsO_{0.8}F_{0.2}$	Ca^{2+}	0.25	0.25	0.138(5)	0.01
	Nd^{3+}	0.25	0.25	0.13(85)	0.99
	Fe^{2+}	0.75	0.25	0.5	1
	As	0.25	0.25	0.657	1
	O^{2-}	0.75	0.25	0	0.8
	F^{-}	0.75	0.25	0	0.2
$NdFeAs_{0.95}Sb_{0.05}O_{0.8}F_{0.2}$	Nd^{3+}	0.25	0.25	0.1385	1
	Fe^{2+}	0.75	0.25	0.5	1
	As	0.25	0.25	0.657	0.95
	Sb	0.25	0.25	0.657	1
	O^{2-}	0.75	0.25	0	0.8
	F^{-}	0.75	0.25	0	0.2
Sample	Structural parameters after refinement				
	Ions	Position			Occupancy
		x	y	z	
$NdFeAsO_{0.8}F_{0.2}$	Nd^{3+}	0.25	0.25	0.138(1)	0.99(8)
	Fe^{2+}	0.75	0.25	0.5	1
	As	0.25	0.25	0.65(8)	0.96(7)
	O^{2-}	0.75	0.25	0	0.8
	F^{-}	0.75	0.25	0	0.2
$Nd_{0.99}Ca_{0.01}FeAsO_{0.8}F_{0.2}$	Ca^{2+}	0.25	0.25	0.138(9)	0.01(1)
	Nd^{3+}	0.25	0.25	0.13(72)	0.98(6)
	Fe^{2+}	0.75	0.25	0.5	1
	As	0.25	0.25	0.657	1
	O^{2-}	0.75	0.25	0	0.8
	F^{-}	0.75	0.25	0	0.2
$NdFeAs_{0.95}Sb_{0.05}O_{0.8}F_{0.2}$	Nd^{3+}	0.25	0.25	0.1385	1
	Fe^{2+}	0.75	0.25	0.5	1
	As	0.25	0.25	0.656	0.86(8)
	As	0.25	0.25	0.656	0.04(9)
	O^{2-}	0.75	0.25	0	0.8
	F^{-}	0.75	0.25	0	0.2

Furthermore, based on the results in Table 3, the "α" and "β" bond angles increase and decrease by substitution of the doped ions, respectively. This is leading to compression of the Fe-As layer, so the lattice parameter "c" and cell volume reduce.

The FeAs4-tetrahedrons play an important role in the crystal structure of RE-1111 compounds. T. Nomura et al. [23] investigated the effect of distortion of the FeAs4 tetrahedron from the regular value

(α=β=109.47°) on the T_C variations. C.H. Lee et al. [24] stated that T_C for IBs reduces by moving away from the regular tetrahedron value.

Table 3. The parameters for the calculation of pattern fitness for the synthesized samples.

Composition	R_{wp} (%)	R_p (%)	R_{exp} (%)	S
$NdFeAsO_{0.8}F_{0.2}$	4.55(3)	3.48(0)	3.91(8)	1.16(2)
$Nd_{0.99}Ca_{0.01}FeAsO_{0.8}F_{0.2}$	6.00(1)	4.64(3)	3.21(4)	1.86(7)
$NdFeAs_{0.95}Sb_{0.05}O_{0.8}F_{0.2}$	5.40(2)	3.98(4)	3.56(9)	1.51(3)

The β angles for our samples versus the β angle for regular FeAs4-tetrahedron are:

$$\beta_{\text{regular FeAs4-tetrahedron}}(109.47°) > \beta_{\text{Nd-1111}}(108.61°) > \beta_{\text{Nd-Ca0.01}}(108.42°) > \beta_{\text{Nd-Sb0.05}}(108.26°)$$

Therefore, it can be anticipated that the superconductivity transition temperature for our pure sample is greater than the others.

3.2 Morphological study

The FE-SEM images of the Nd-1111, Nd-Sb0.05 and Nd-Ca0.01 samples have been shown in Figures 4 (a)-(c). It is evident from these figures that the grains are randomly oriented. In addition, the presence of the sharp-edge grains indicate the high accuracy in choosing the important temperatures in the production of our samples.

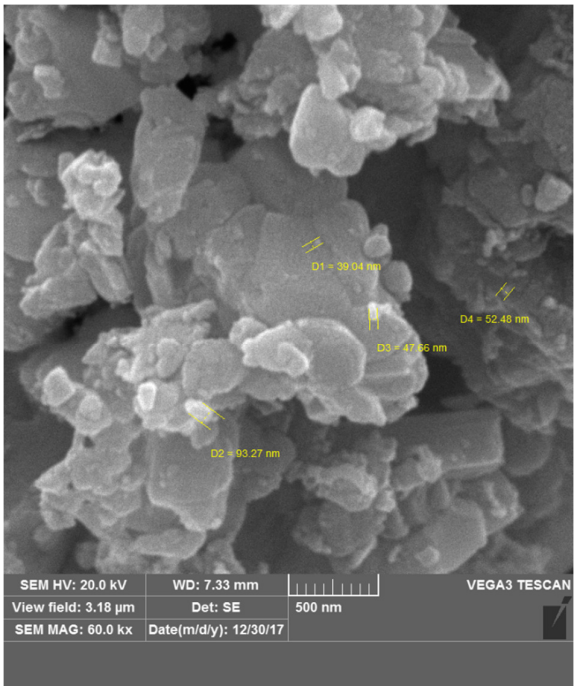

Figure 4- a. SEM image for Nd-1111.

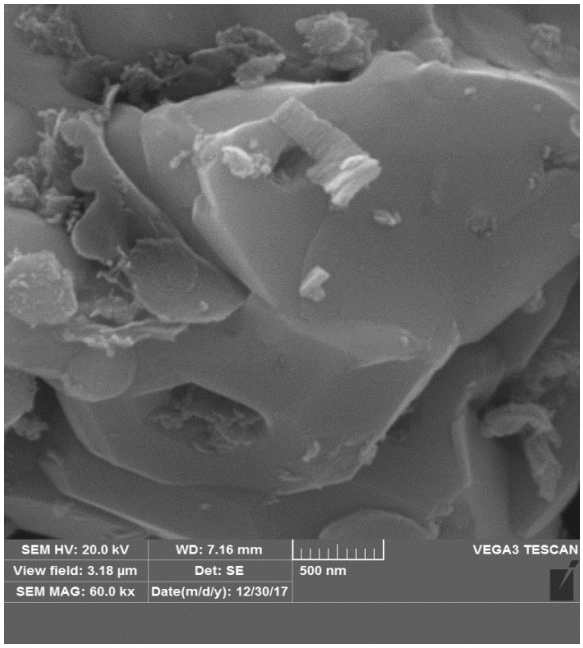

Figure 4- b. SEM image for Nd-Sb0.05.

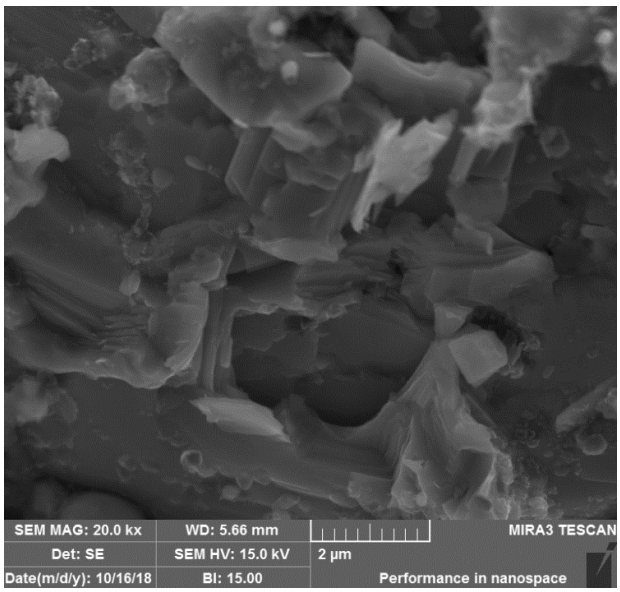

Figure 4- c. SEM image for Nd-Ca0.01.

3.3 Electrical measurement

The effect of Ca/Nd and Sb/As doping on the electrical properties of the synthesized samples is studied through resistivity measurements by the 4-prob technique. The temperature dependence of R/R_{300K} for our synthesized samples is displayed in Figure 5. For the Nd-1111 sample, the electrical resistivity gradually drops by decreasing temperature before the superconductivity transition occurs at $T_C^{mid} = 56K$.

For the Nd-Sb0.05 sample, the electrical resistivity decreases by cooling before dropping rapidly at T_{onset}=48 K, which finally reaches zero at T_{offset}=44 K [25]. The critical temperature was obtained at 46 K for this sample. This sample has a metallic behavior similar to the pure sample up to the room temperature. The Nd-Ca0.01 sample represents the structural transition (T_S) at T_S=125K before the electrical resistivity slowly decreases by cooling. The superconductivity transition of this sample happens at $T_C^{mid} = 48K$ [26]. The existence of structural transition suggests that the superconductivity appears in the orthorhombic phase, as reported in ref. [23]. It seems that T_C decreases by substitution of Ca/Nd and

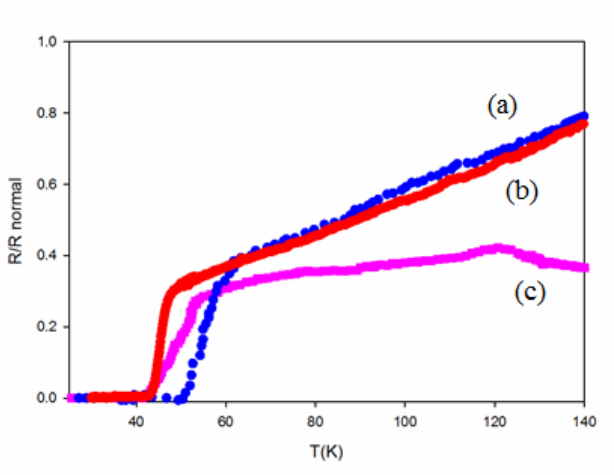

Figure 5. The normalized resistivity of (a) Nd-1111(blue line), (b) Nd-Sb0.05(red line) and (c) Nd-Ca0.01 (pink line).

Sb/As. By comparing the results obtained from our structural and electrical measurements, it can be understood that T_C decreases with increasing the relative distortion of FeAs4-tetrahedrons from the regular ones, see Table 4. Our results are in good agreement with T. Nomura et al. [23] and C.H. Lee et al. [24]. Our Result about the variation of T_C versus the α, β and the bound length of Fe-As for Nd-1111, Nd-Ca0.01 and Nd-Sb0.05 samples are shown in Figures 6a-6c. Our data shown in Table 4 and Figures 6a-6c represents the three following points, regardless of the doping type and site of substitution:

1. T_C decreases with decreasing of Fe-As bond length.
2. T_C decreases with increase of α and decrease of β bond angles of FeAs4-tetrahedrons from regular ones.
3. The two above items cause the lattice parameter "c" contraction.

Finally, this confirms the theoretical results of K. Kuroki et al. [27, 28].

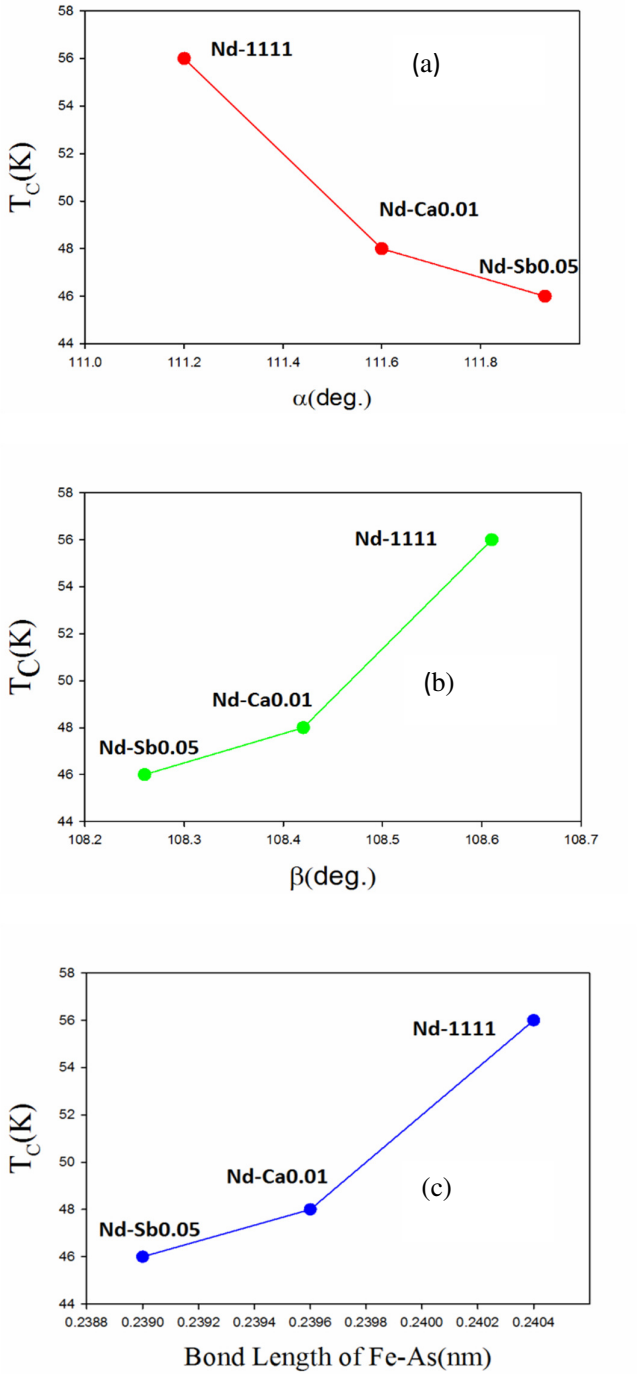

Figure 6. The variation of T_C versus (a) the α, (b) the β and (c) the bond length of Fe-As for our samples.

Therefore, it is significant that there is a relation between the structural properties and superconductivity in our samples. Also, based on our experimental investigation, the relation is independent from the doping type whether the substitution is in the superconductive planes or in the layer of charge reservoirs.

Table 4. The crystal structure such as Lattice parameters, cell volume, bond length, bond angle, thickness of Fe-As and Nd-(O/F)-Nd layers and T_C.

Sample	Lattice Parameters		Cell Volume Å³	Bond Length (Å)	
	a(Å)	c(Å)		Fe-As	Nd-(O/F)
Nd-1111	3.96(7)	8.59(6)	135.27(6)	2.404(3)	2.316(4)
Nd-Ca0.01	3.96(4)	8.55(8)	134.47(4)	2.396(4)	2.309(4)
Nd-Sb0.05	3.96(2)	8.56(0)	134.37(0)	2.390(3)	2.340(4)

Sample	Bond angle (°)			$T_c(K)$
	As-Fe-As		(O/F)-Nd-(O/F)	
	α	β		
Nd-1111	111.20(1)	108.61(6)	117.8(2)	56
Nd-Ca0.01	111.60(7)	108.42(4)	117.13(8)	48
Nd-Sb0.05	111.93(1)	108.26(6)	115.6(2)	46

Sample	Thickness of Fe-As layer (Å)	Thickness of Nd-(O/F) layer (Å)
Nd-1111	2.71(6)	2.41(8)
Nd-Ca0.01	2.61(9)	2.40(8)
Nd-Sb0.05	2.67(5)	2.49(2)

4 Conclusions

In summary, we report the highest superconductivity transition temperature for nominal composition $NdFeAsO_{0.8}F_{0.2}$ sample is 56K. In this paper, the effect of doping in FeAs and Nd-(O/F) layers were studied with the Rietveld's refinement of XRD data by the MAUD software. We found that:

1- A small value of the Sb or Ca doping markedly reduced Tc. The superconductivity transition temperature of Nd-Sb0.05 and Nd-Ca0.01 is 48K and 46 K, respectively.
2- Based on XRD data analysis, the distortion of "β" angle increases from FeAs4-tetrahedron with the doping of Sb/As and Ca/Nd in the pure sample that causes reduce in the superconductivity transition temperature of the 1111 structure.
3- T_C decreases with decreasing the Fe-As bond length.
4- T_C decreases with the increase of α and decrease of β bond angles of FeAs4-tetrahedrons from regular ones.
5- The third and fourth items cause the lattice parameter "c" contraction.
6- The above relation is independent from the doping type and whether the substitution is in the superconductive planes or in the layer of charge reservoirs.

Acknowledgments

The authors wish to thank for financial support of the vice chancellor research and technology of Alzahra university.

References

[1] H.H. Yoichi Kamihara, M. Hirano, R. Kawamura, H. Yanagi,T. Kamiya, H. Hosono, Iron-Based Layered Superconductor: LaOFeP Journal of American Chemical Society, **128** (2006) 10012.

[2] T.W. Yoichi Kamihara, M. Hirano, H. Hosono, "Iron-Based Layered Superconductor La[$O_{1-x}F_x$]FeAs(x=0.05-0.12) with Tc=26K." Journal of American Chemical Society, **130** (2008) 3296.

[3] J. G. Bednorz, K. A. Müller, "Possible High Tc Superconductivity in the Ba - La- Cu- O, System Z." Physica B: Condensed Matter, **64** (1986) 189.

[4] S. Gholipour, V. Daadmehr, A.T. Rezakhani, H. Khosroabadi, F. Shahbaz Tehrani, R. Hosseini Akbarnejad, "Structural Phase of Y358 Superconductor Comparison with Y123." Journal of Superconductivity and Novel Magnetism, **25** (2012) 2253.

[5] H. Takahashi, K. Igawa, K. Arii, Y. Kamihara, M. Hirano, H. Hosono, "Superconductivity at 43 K in an iron-based layered compound $LaO_{1-x}F_xFeAs$." Nature, **453** (2008) 376.

[6] H.H. Nan-Lin Wang, P. Dai, "Iron based superconductor." Taylor & Francis Group, LLC, Broken Sound Parkway NW, 2013.

[7] F.C. Hsu, J.Y. Luo, K.W. Yeh, T.K .Chen, T.W. Huang, P.M. Wu, Y.C. Lee, Y.L. Huang, Y.Y. Chu, D.C. Yan, M.K. Wu, "Superconductivity in the PbO-type structure alpha-FeSe." Proceedings of the National Academy of Sciences of the United States of America, **105** (2008) 14262.

[8] J.H. Tapp, Z. Tang, B. Lv, K. Sasmal, B. Lorenz, P.C.W. Chu, A.M. Guloy, "LiFeAs: An intrinsic FeAs-based superconductor withTc=18 K." Physical Review B, **78** (2008) 060505.

[9] M. Rotter, M. Tegel, D. Johrendt, "Superconductivity at 38 K in the iron arsenide ($Ba_{1-x}K_x$)Fe_2As_2." Physical Review Letters, **101** (2008) 107006.

[10] F. Hardy, R. Eder, M. Jackson, D. Aoki, C. Paulsen, T. Wolf, P. Burger, A. Böhmer, P. Schweiss, P. Adelmann, R.A. Fisher, C. Meingast, "Multiband Superconductivity in KFe_2As_2: Evidence for One Isotropic and Several Lilliputian Energy Gaps." Journal of the Physical Society of Japan, **83** (2014) 014711.

[11] M. Calamiotou, D. Lampakis, N.D. Zhigadlo, S. Katrych, J. Karpinski, A. Fitch, P. Tsiaklagkanos, E. Liarokapis, "Local lattice distortions vs. structural phase transition in $NdFeAsO_{1-x}F_x$." Physica C: Superconductivity and its Applications, **527** (2016) 55.

[12] Y .Qi, Z. Gao, L. Wang, D. Wang, X. Zhang, Y. Ma, "Superconductivity in Co-doped SmFeAsO." Superconductor Science and Technology, **21** (2008) 115016.

[13] J. Dong, H.J. Zhang, G. Xu, Z. Li, G. Li, W.Z. Hu, D. Wu, G.F. Chen, X. Dai, J.L. Luo, Z. Fang, N.L. Wang, Competing orders and spin-density-wave instability in $La(O_{1-x}F_x)FeAs$, Europhysics Letters, **83** (2008) 27006.

[14] H. Ota, K. Kudo, T. Kimura, Y. Kitahama, T. Mizukami, S. Ioka, M. Nohara, "Site-Selective Antimony Doping in Arsenic Zigzag Chains of 112-Type $Ca_{1-x}La_xFeAs_2$." Journal of the Physical Society of Japan, **86** (2017) 025002.

[15] F. Ye, S. Chi, W. Bao, X.F. Wang, J.J. Ying, X.H. Chen, H.D. Wang, C.H. Dong, M. Fang, "Common crystalline and magnetic structure of superconducting $A_2Fe_4Se_5$ (A=K,Rb,Cs,Tl) single crystals measured using neutron diffraction." Physical Review Letters, **107** (2011) 137003.

[16] Z. Alborzi, V. Daadmehr, "Synthesis and characterization of iron based superconductor Nd-1111." Physica C: Superconductivity and its Applications, **549** (2018) 116.

[17] R S Meena, K.V.R.Rao, H. Kishan, V. P. S. Awana, "Inter-comparison of electric and magnetic behaviour of superconducting quaternary oxypnictide compounds." IOP Conference Series: Materials Science and Engineering, **171** (2017) 012153.

[18] P.M. Aswathy, J.B. Anooja, N. Varghese, C.K. Chandrakanth, N. Devendra Kumar, A. Sundaresan, U. Syamaprasad, "Rare earth (RE – Ce, Gd) modified $Nd_{1-x}RE_xFeAsO_{0.7}F_{0.3}$superconductor with enhanced magneto-transport properties." RSC Advances, **5** (2015) 41484.

[19] S. Chul Lee, E. Satomi, Y. Kobayashi, M. Sato, "Effects of Ru Doping on the Transport Behavior and Superconducting Transition Temperature of $NdFeAsO_{0.89}F_{0.11}$." Journal of the Physical Society of Japan, **79** (2010) 023702.

[20] P.M. Aswathy, J.B. Anooja, N. Varghese, U. Syamaprasad, "Microstructural refinement and enhanced transport properties in binary doped NdFeAsO superconductor." Journal of Applied Physics, **115** (2014) 053903.

[21] A. Kawabata, S. Chul Lee, T. Moyoshi, Y. Kobayashi, M. Sato, "Superconductivity of $LaFe_{1-y}Co_yAsO_{1-x}F_x$." Journal of the Physical Society of Japan, **77** (2008) 103704.

[22] K.D.S.a.C.K. Jorgensen, "Electronegativity." Springer-Verlag, Berlin, Heidelberg, NewYork, 1967.

[23] T. Nomura, Y. Inoue, S. Matsuishi, M. Hirano, J. E. Kim, K. Kato, M. Takata, H. Hosono, "Comparison of crystal structures and the effects of Co substitution in a new member of the Fe-1111 superconductor family AeFeAsF (Ae = Ca and Sr): a possible candidate for a higher-*T*c superconductor." Superconductor Science and Technology, **22** (2009) 055016.

[24] C.-H. Lee, A. Iyo, H. Eisaki, H. Kito, M. Teresa Fernandez-Diaz, T. Ito, K. Kihou, H. Matsuhata, M. Braden, K. Yamada, "Effect of Structural Parameters on Superconductivity in Fluorine-Free $LnFeAsO_{1-y}$(Ln = La, Nd)." Journal of the Physical Society of Japan, **77** (2008) 083704.

[25] Z. Alborzi and V. Daadmehr, Journal of Superconductivity and Novel Magnetism, submitted , https://arxiv.org/abs/1901.00797v1 (2019).

[26] F.S. Tehrani and V. Daadmehr, https://arxiv.org/abs/1901.10872v1(2019).

[27] K. Kuroki, H. Usui, S. Onari, R. Arita, H. Aoki, "Pnictogen height as a possible switch between high-*Tc* nodeless and low-*Tc* nodal pairings in the iron-based superconductors." Physical Review B, **79** (2009) 224511.

[28] K. Kuroki, "Anion height as a controlling parameter for the superconductivity in iron pnictides and cuprates." Journal of Physics and Chemistry of Solids, **72** (2011) 307.